Local work function Moiré pattern on ultrathin ionic films: NaCl on Ag(100)

Marina Pivetta,[1] François Patthey,[1] Massimiliano Stengel,[2,*] Alfonso Baldereschi,[2] and Wolf-Dieter Schneider[1]
[1]*Ecole Polytechnique Fédéralede Lausanne (EPFL), Institut de Physique des Nanostructures, CH-1015 Lausanne, Switzerland*
[2]*Ecole Polytechnique Fédérale de Lausanne (EPFL), Institut Romand de Recherche Numérique en Physique des Matériaux (IRRMA) and Institute of Theoretical Physics, CH-1015 Lausanne, Switzerland*
(Received 7 July 2005; published 2 September 2005)

In the submonolayer island growth of NaCl on Ag(100) two orientations, 0° and 45°, of the NaCl unit cell with respect to the substrate are observed by scanning tunneling microscopy. For the latter we observe a pronounced Moiré pattern, which we assign to a modulation of the local work function, as deduced by tunneling spectroscopy of image-potential states. First-principles calculations elucidate the charge-transfer mechanisms responsible for the local work function corrugation and give indications on the local relative position of the NaCl molecules with respect to the substrate.

DOI: 10.1103/PhysRevB.72.115404 PACS number(s): 68.55.Ac, 68.37.Ef

I. INTRODUCTION

Moiré patterns are intriguing phenomena generated by the superposition of two periodic structures with small lattice mismatch, which have been observed, e.g., by scanning tunneling microscopy (STM), on layered materials such as graphite[1] or transition-metal dichalcogenides[2,3] and on thin films.[4–7] Their interpretation is not straightforward and requires a profound knowledge of the surface properties. The relationship, at the atomic scale, between these patterns and the local density of electronic states of the supported film, which is probed by STM, is not yet clear.

For Ag films grown on Cu(111), a shift of the Ag surface state has been observed and associated with a Moiré superstructure.[4] For Pb islands on Si(111), a Moiré pattern has been related to the spatial modulation of the potential confining the electrons in the Pb film.[5] Ultrathin NaCl layers on Cu(111) modify the substrate electronic structure and produce a Moiré pattern which has been attributed to a gap opening in the surface-state band.[6] A Moiré pattern has been observed for the local tunneling barrier height of monolayer graphite on Pt(111) and tentatively related to a spatial modulation of the local work function.[7]

In this paper we demonstrate the existence of a local work function Moiré for ultrathin NaCl films on Ag(100) using STM, scanning tunneling spectroscopy (STS), and density-functional theory (DFT) calculations. We also discuss the local relative position of the NaCl molecules with respect to the substrate atoms.

II. EXPERIMENTAL

The experiments were performed in a homebuilt low-temperature STM.[8] The Ag(100) single crystal was cleaned by standard sputtering and annealing cycles. NaCl was evaporated from a Knudsen effusion cell, with the substrate temperature during deposition [0.2 monolayer (ML)/min] ranging between room temperature and 500 K. The tunneling measurements were carried out at 50 K, using a cut PtIr tip. Bias voltages V refer to the sample voltage with respect to the tip, and all STM images were acquired in constant current mode. Differential conductance (dI/dV) spectra were measured by lock-in detection in closed-loop conditions.

III. RESULTS AND DISCUSSION

Figure 1(a) shows a typical 400×400 nm^2 STM image measured on NaCl/Ag(100), where the NaCl nominal coverage is 1 ML. The islands have an average size of 50 nm and a typical thickness of 1 ML (most have a partial second layer). The Ag steps act as nucleation sites for the first and for the following layers, and the NaCl islands extend symmetrically on both sides of the steps. Figure 1(b) shows an atomically resolved image of the clean Ag(100) surface. Figure 1(c) presents an image obtained on 1 ML NaCl/Ag(100), where only the Cl ions are imaged as protrusions.[9] The NaCl and Ag surface unit cells have the same orientation (0° growth),[10,11] with a weak mosaicity (±7°), and the NaCl island borders are oriented along the [010] and [001] directions, in order to insure nonpolar edges. Contrary to the interpretation reported in the literature,[10,11] we find that the growth orientation is not determined by the substrate step direction and, moreover, that NaCl islands nucleate with 0° orientation also on terraces.[12]

An intriguing island can be seen at the bottom right corner of Fig. 1(a): it is oriented at about 45° with respect to the average direction of the other islands. The atomic orientation of its unit cell must also be different in order to insure nonpolar edges. Indeed, Fig. 1(d) shows an atomically resolved image of this island, where the NaCl unit cell is oriented at 45° with respect to the one shown in Fig. 1(c) and the one measured on the substrate, Fig. 1(b). Islands with 45° orientation always nucleate at steps and their number is $<5\%$ of the total.

Figure 2(a) shows a 300×300-nm^2 STM image measured on a sample with 1 ML NaCl nominal coverage, in which large islands with both 0° and 45° orientation are present. For the islands with 0° orientation, which have a large (38%) lattice mismatch with the Ag substrate, we occasionally observe a weak Moiré pattern with a periodicity as small as 1.2 nm and a corrugation below 10 pm, as the one shown in Fig.

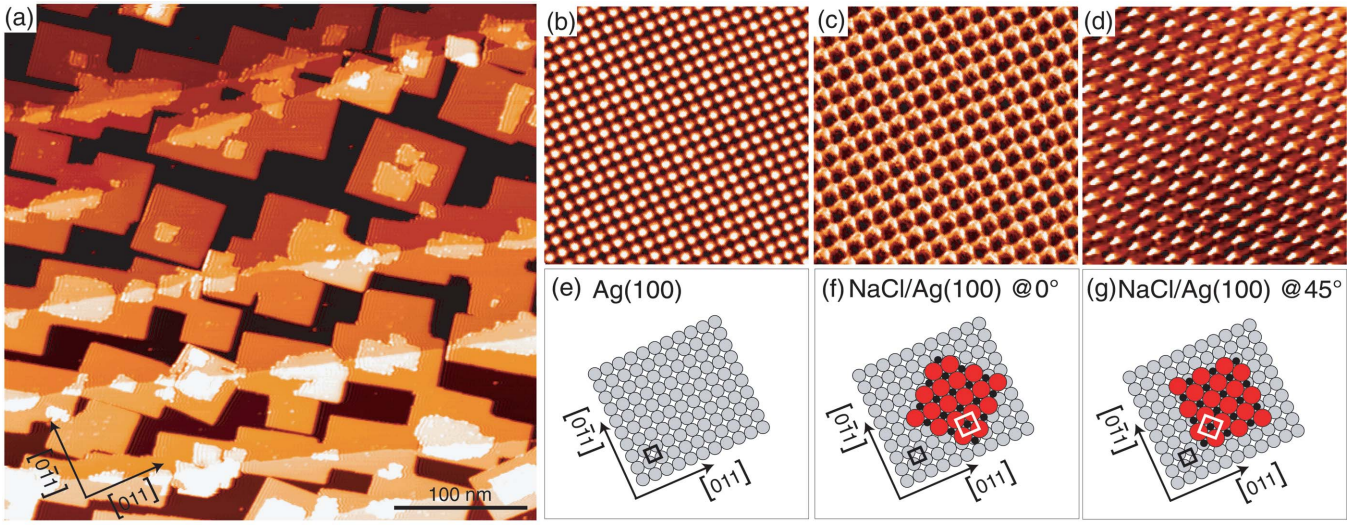

FIG. 1. (Color) (a) STM image on NaCl/Ag(100) (400×400 nm^2, $V=+4.18$ V, $I=20$ pA). (b)–(d) STM images (5.6×5.6 nm^2) showing atomic resolution on Ag(100) ($V=-20$ mV, $I=50$ pA), 1 ML NaCl/Ag(100) @ 0° ($V=-110$ mV, $I=20$ pA), 1 ML NaCl/Ag(100) @ 45° ($V=-100$ mV, $I=23$ pA). (e)–(g) Schematic representation of Ag(100) and NaCl adlayer, showing the high-symmetry directions, the unit cells, and the island orientation.

2(b). However, the weakness of these superstructures prevents any quantitative investigation.

The patterns measured on the islands grown at 45°, on the contrary, can be analyzed in detail taking advantage of their intensity and large periodicity. On the island with 45° orientation that can be seen in Fig. 2(a), a superstructure with a periodicity of approximately 7.8 nm and a bias-dependent corrugation of up to 2 Å is visible. The pattern changes contrast on successive NaCl layers. Figures 2(c) and 2(d) present two images, acquired on the same region at $V=+3.25$ V and +20 mV, respectively. In Fig. 2(d) the Moiré pattern and the atomic resolution of the NaCl adlayer are displayed simultaneously. The periodicity of the pattern shown in Fig. 2(c) corresponds exactly to the one observed at lower bias voltage in Fig. 2(d), and thus we associate the superstructure observed at high bias voltages to the Moiré pattern, i.e., to the adlayer-substrate lattice mismatch.

Several values of the Moiré periodicity, ranging from 6 to 8.5 nm, have been observed, the latter corresponding to a 3.3% lattice mismatch between the Ag substrate and the NaCl film, i.e., a 0.8% contraction of the adsorbed monolayer lattice constant with respect to the NaCl bulk value. Smaller values of the Moiré periodicity might be caused by a rotation of the NaCl adlayer (a few degrees strongly affect the Moiré periodicity) and/or a larger contraction of the NaCl film.

Figure 2(e) shows the tip displacenent z (top panel) and simultaneously acquired dI/dV values (bottom panel) as a function of bias on the clean Ag(100) surface and on the NaCl/Ag(100) system. Figure 2(f) shows the same quantities measured on the regions A (bright) and B (dark), indicated in Fig. 2(c). The structures observed in the $z(V)$ curves and in the dI/dV spectra originate from image-potential states, i.e., unoccupied states which are bound by the classical image-charge response of the metallic surface and have a free-electron-like dispersion parallel to it.[13–15] In the $z(V)$ curves, the contribution of each image-potential state appears as a step (corresponding to a tip displacement), while in the dI/dV spectra well defined peaks are observed. In STS the Stark effect shifts and expands the energy spectrum of image-potential states.[16] Nevertheless, significant knowledge can be gained by comparing spectra, in particular those acquired on different regions of one given sample.[17–21] In Fig. 2(e), we identify the first image-potential state for the clean Ag surface at +4.3 V, while for 1 ML NaCl it is found at +3.1 V, i.e., at a considerably lower bias. This large bias difference is related to (but, in view of the Stark effect and of the different surface composition, is not a measure of) the expected reduction of the work function of the clean Ag(100) surface upon adsorption of an insulating layer.[6,22–25] In Fig. 2(f), the image-potential states measured on bright regions (A) are found at lower bias than those acquired on dark regions (B). From the data, the difference of the lowest image potential states between regions A and B is $\approx$0.15 V. Moreover, the spectral width of the states is different, indicating a longer lifetime for states corresponding to the bright regions. Thus the STM contrast observed between regions A and B in Fig. 2(c) originates from the energy shift of the ground state of the image-potential spectrum, while the contrast in Fig. 2(a) is due to the shift of the first-excited image-potential state. The applied electric field amplifies the energy differences by stretching the spectra[16] but, given that the measurements are performed at identical tip conditions on different areas of one Moiré pattern, the energy shifts of the image potential states are bona fide fingerprints of differences of the local work function between regions A and B. A decrease of the local work function determines a shift of the image-potential states towards lower energies[24,25] (i.e., they are observed at lower bias in the STS spectra), and therefore we conclude that the local work function corresponding to region A of the Moiré pattern is lower than that corresponding to region B.

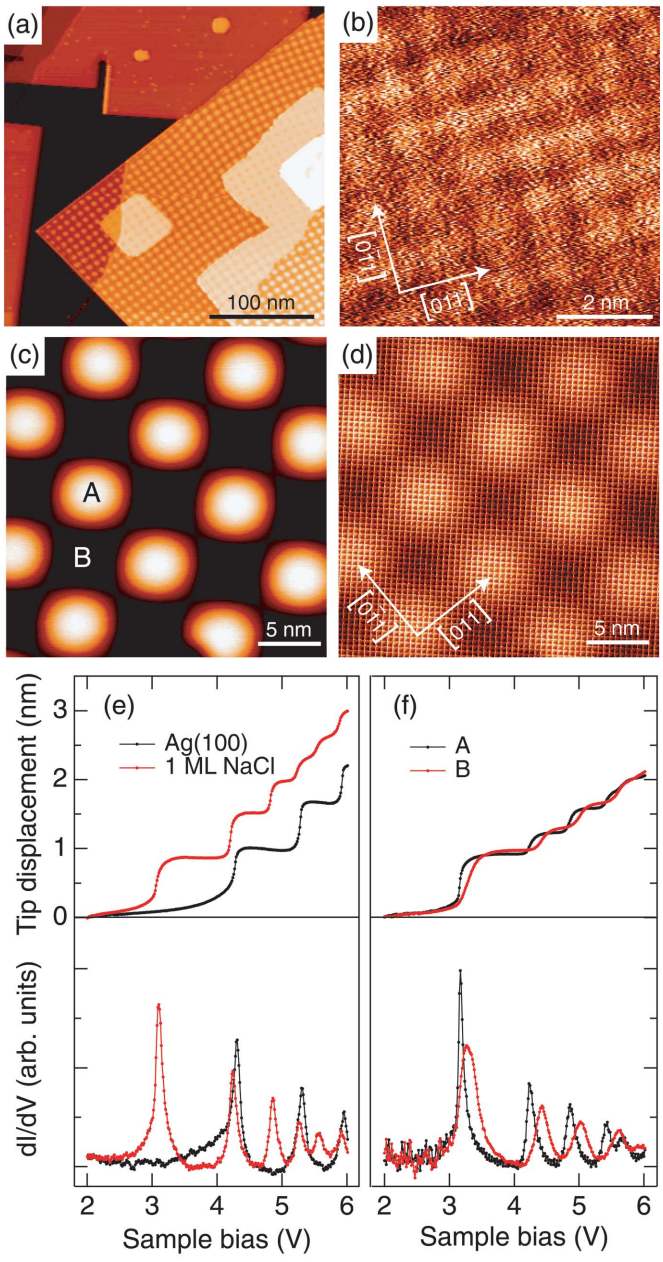

FIG. 2. (Color) (a) STM image showing NaCl islands grown with 0° and 45° orientation (300×300 nm^2, $V=+4.15$ V, $I=20$ pA). (b) STM image acquired on a 0° island (5×5 nm^2, $V=+3$ V, $I=20$ pA). The Ag(100) crystallographic directions are indicated. (c), (d) STM images acquired on a 45° island (25×25 nm^2), (c) $V=+3.25$ V, $I=20$ pA, (d) $V=+20$ mV, $I=500$ pA. The Ag(100) crystallographic directions are indicated. (e), (f) $z(V)$ curves (top) and dI/dV spectra (bottom) (closed-feedback loop, $V_0=+2.0$ V, $I=20$ pA, modulation amplitude: 5 mV) acquired on (e) Ag(100) and 1-ML NaCl and (f) 1-ML NaCl grown at 45° on regions A and B indicated in (c).

In order to support the interpretation of the observations on the islands with 45° orientation in terms of a modulation of the local work function, we have calculated the structural and electronic properties of free and Ag(100) supported NaCl monolayers. The computations are performed within density-functional theory (DFT), using the generalized gradient approximation (GGA) with the PW91 functional for exchange and correlation[26] and the projector augmented-wave (PAW) method.[27] For the unsupported NaCl monolayer we calculate an in-plane lattice constant of 5.45 Å, i.e., 4.4% smaller than the theoretical lattice parameter of bulk NaCl (5.70 Å). The compression (with repect to bulk NaCl) calculated for the *unsupported* monolayer is much larger than that ($\approx1\%$) experimentally measured for the *adsorbed* film. Considering that the computational scheme provides lattice parameters with an accuracy of 1% or better, the compressional values given above indicate that the interaction between the Ag substrate and the NaCl adlayer increases the lattice constant of the latter.

A direct calculation of the modulation of the local work function and of the binding-energy dispersion of the image-potential states would be too demanding, since it would require an exceedingly large supercell. We study therefore pseudomorphic NaCl overlayers, artificially expanded to match the Ag(100) substrate with a $(\sqrt{2}\times\sqrt{2})R45°$ periodicity. We investigate two different adsorption geometries (*atop* and *hollow*) which are representative of the two extreme configurations of the real system. For each geometry, both Cl and Na occupy the same kind of adsorption site (*atop* or *hollow*), as sketched in Figs. 3(d) and 3(e).

The Ag(100) surface is modeled with periodically repeated nine-layer Ag slabs separated by a vacuum region with thickness ≈15 Å. The in-plane lattice parameter of the slabs has been set to the calculated lattice constant of bulk Ag (4.19 Å). NaCl is adsorbed on both sides of the slabs to avoid macroscopic electric fields in the vacuum region. A set of six special points corresponding to a 8×8 Monkhorst-Pack mesh in the 1×1 Ag(100) surface unit cell is used for Brillouin-zone integrations, with a Fermi-Dirac smearing of 0.25 eV. Electronic and atomic relaxations are performed with a modified Car-Parrinello method.[29]

The calculated adsorption energies E_{ads} (Table I) for the two geometries are small and close to each other, indicating weak physisorption and negligible site preference. These values are smaller than those reported for NaCl on Cu(100) (≈0.25 eV),[30] and hint to a weaker interaction of the NaCl film with the less reactive Ag surface, as expected. The calculated strain energy necessary to expand the NaCl adlayer to match the Ag lattice constant is 0.15 eV, much larger than the adsorption energy difference between the two sites (0.03 eV). The latter energy would not compensate the strain energy necessary to have a NaCl layer in registry with the substrate. This result corroborates the picture of a NaCl film growing incommensurate to the substrate without any significant stress modulation. The calculated work functions indicate, as expected, a substantial lowering of the Ag(100) value (4.36 eV) upon adsorption of the dielectric film in either geometry. Strikingly, despite the relatively weak interaction between the NaCl film and the substrate and the weak site dependence of the adsorption energy, the difference in work function between *atop* and *hollow* configurations is large ($\Delta W=0.38$ eV).

In order to separate electronic and ionic contributions to the work function difference ΔW, we first calculate the induced charge density for a flat NaCl monolayer positioned at

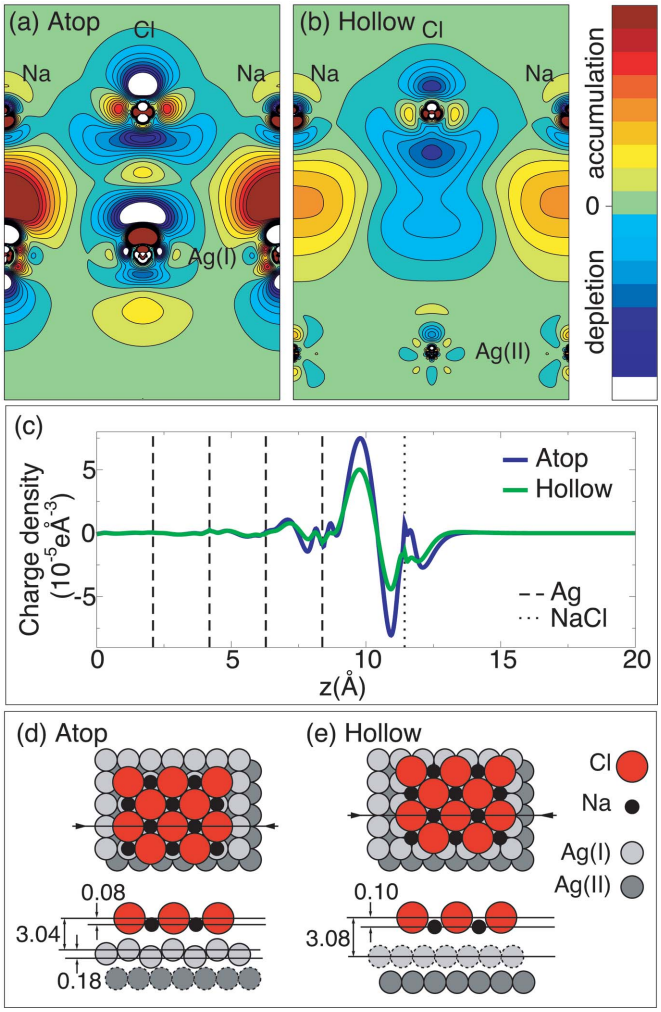

FIG. 3. (Color) Induced charge-density contours (vertical cutplane passing through a neighboring Na-Cl pair) for a flat NaCl monolayer adsorbed on unrelaxed Ag(100); (a) *atop* and (b) *hollow* site; Ag(I) and (II) indicate Ag atoms of the first and second layer, respectively. (c) induced charge-density average on *xy* planes parallel to the surface. (d), (e) Top view of the two adsorption geometries; vertical cuts showing the relaxed geometry for the two configurations (distances in Å, vertical atomic displacements not to scale for better evidencing the salient features), dashed contours indicate Ag atoms which do not lie in the cutplane.

a fixed distance of 3.05 Å from the ideal (unrelaxed) Ag surface. The results shown in Figs. 3(a) and 3(b) indicate that for both geometries there is an important depletion of the Cl $3p_z$ orbitals, the electronic charge being transferred towards the substrate and in particular to the interfacial region between the Na ions and the outermost Ag layer. The overall rearrangement of electronic charge is larger for the *atop* geometry, in which case a weak covalent bonding develops between the Cl ion and the facing, outermost Ag atom (local maximum at the midpoint). This induced charge modifies the surface dipole, determining a substantial lowering of the Ag(100) work function for both geometries (see Table I, values in parentheses) and particularly for the *atop* configuration, where the induced dipole is larger; see Fig. 3(c). When the atoms are allowed to relax, a "rumpling" in the NaCl film appears, with the Cl ions protruding from the surface. This effect is slightly larger for the *hollow* configuration, as shown in Figs. 3(d) and 3(e). Moreover, the outermost Ag layer has an important corrugation in the *atop* geometry (with the Ag atoms facing the Cl ions, protruding from the outer Ag layer and enhancing the weak covalent Ag-Cl bond), while it is flat by symmetry in the *hollow* case. Both relaxation mechanisms concur to increase the difference in the work function from 0.20 eV (flat structures) to the final value $\Delta W = 0.38$ eV.

TABLE I. Adsorption energy E_{ads} and work function of an expanded NaCl monolayer adsorbed pseudomorphically onto the atop and hollow sites of Ag(100) with 45° orientation. Values in parentheses indicate the work function values prior to atomic relaxation (see text). The calculated work function of clean Ag(100) is 4.36 eV.

System	E_{ads} (eV/NaCl unit)	Work function (eV)
Atop	0.13	3.65 (3.47)
Hollow	0.10	4.03 (3.67)

To make contact with experiment, we must investigate the modulation of the structural and electronic properties of the NaCl/Ag(100) system over the large unit cell corresponding to the observed Moiré periodicity. We can estimate these quantities by using the DFT results obtained for the *atop* and *hollow* small unit cells. Several effects must be taken into account when going from the small unit cells to the Moiré supercell. (i) The calculated work function difference ΔW between *atop* and *hollow* geometries will manifest itself in the large unit cell as a nonuniform dipole moment density on the metallic surface which will produce a corrugation $\Delta W/2$ of the local work function in the vacuum and an opposite corrugation $-\Delta W/2$ of the slab potential in the neighborhood of the surface. (ii) The tensile strain of the NaCl overlayer has been exaggerated in our small-unit-cell model with respect to that of the real system, in order to match the surface periodicity of the Ag substrate. This additional strain is likely responsible for enhanced vertical relaxations and charge transfers, i.e., for an overestimation of the local work function modulation $\Delta W/2$ between *atop* and *hollow* regions. (iii) Inhomogeneities will occur within the incommensurate NaCl film, as a consequence of the local competition between site preference and internal stress relaxation. These inhomogeneities might introduce elastic deformations into the system and contribute to the corrugation of the electrostatic potential in vacuum. Considering the stiffness of the overlayer and the weak site dependence of its adsorption energy, this effect is expected to be rather small, and to contribute only weakly to the corrugation of the local work function. (iv) A nonuniform two-dimensional (2D) charge density will appear at the metallic surface, such that the electrostatic potential satisfies the correct boundary conditions away from the interface.[28] This surface charge density will cancel the corrugation of the slab potential (i.e., will cancel the electrostatic fields within the metallic Ag slab) and will enhance the local work function modulation in the vacuum to the calculated work function difference ΔW. (v) The corrugation of the electrostatic potential decreases exponentially in the

vacuum with a decay length $a/2\pi \approx 1.2$ nm, where $a = 7.8$ nm is the in-plane periodicity of the dipole moment density on the surface. (vi) Finally, the structures in the STS spectra are related to the modulation of the local work function, since they correspond to the energy levels of the image-potential spectrum. The corrugation of the local work function will affect the image-potential states (the image-charge potential being the dominant term) by lowering their energy in correspondence to the *atop* regions where the local work function is smaller. A crude estimate of this effect, which neglects potential dispersions parallel to the surface, can be obtained by using the simple 1D model of image-potential states based on an infinite potential barrier at the image plane $z=0$, and an ideal $V(z)=-1/4z$ potential in the vacuum region. The ground state of this model has a hydrogenic, exponential wave function and energy $\epsilon = -\frac{1}{16}\mathrm{Ry}$. The effects of the corrugation of the local work function ΔW can then be obtained by first-order perturbation theory, which leads roughly to a corrugation of $0.77\Delta W \sim 0.29$ eV for the "local energy" of the ground image-potential state. A more quantitative comparison between theory and experiment would require a reliable calculation of the excited states at the surface, which would be prohibitive to perform *ab initio*, even for the pseudomorphic structures with small unit cell.

IV. SUMMARY

A qualitative picture of the relevant physics has been achieved, in spite of the discrepancy between the experimental data and the theoretical estimate. The calculations demonstrate that the NaCl adlayer strongly reduces the work function of the Ag(100) surface and quite different dipole moment densities occur at the surface in correspondence to the *atop* and *hollow* regions. This results in a strong modulation of the local work function, in agreement with the observed pronounced energy shift of the image-potential states. The calculated local work function is lower in the *atop* geometry than in the *hollow* one, indicating that the bright regions A in the STM images should correspond to *atop* adsorption regions for the NaCl molecules.

Before closing, we would like to emphasize that the mechanisms here proposed for the interpretation of the data on the NaCl islands with 45° orientation apply equally well to the 0° oriented islands. In this case, however, the strong lattice mismatch (38%) with the Ag substrate will result in a smaller corrugation of the local work function. Furthermore, given the short Moiré periodicity $a=1.2$ nm, the modulation of the local work function will decrease exponentially in the vacuum with a decay length $a/2\pi \approx 0.2$ nm. A local work function corrugation which is weaker and extends much less in vacuum will have a much smaller effect on the energy of the image-potential states in agreement with the weakness of the STM superstructures observed on these islands.

ACKNOWLEDGMENTS

This work was supported by the Swiss National Science Foundation.

*Present address: Materials Department, University of California, Santa Barbara, CA 93106-5050.

[1] Z. Y. Rong and P. Kuiper, Phys. Rev. B **48**, 17427 (1993).
[2] B. A. Parkinson, F. S. Ohuchi, K. Ueno, and A. Koma, Appl. Phys. Lett. **58**, 472 (1991).
[3] K. Kobayashi, J. Vac. Sci. Technol. B **14**, 1075 (1996); Phys. Rev. B **53**, 11091 (1996).
[4] A. Bendounan, H. Cercellier, Y. Fagot-Revurat, B. Kierren, V. Y. Yurov, and D. Malterre, Phys. Rev. B **67**, 165412 (2003).
[5] W. B. Jian, W. B. Su, C. S. Chang, and T. T. Tsong, Phys. Rev. Lett. **90**, 196603 (2003).
[6] J. Repp, G. Meyer, and K.-H. Rieder, Phys. Rev. Lett. **92**, 036803 (2004).
[7] M. Sasaki, Y. Yamada, Y. Ogiwara, S. Yagyu, and S. Yamamoto, Phys. Rev. B **61**, 15653 (2000).
[8] R. Gaisch, J. K. Gimzewski, B. Reihl, R. R. Schlittler, M. Tschudy, and W.-D. Schneider, Ultramicroscopy **42-44**, 1621 (1992).
[9] W. Hebenstreit, J. Redinger, Z. Horozova, M. Schmid, R. Podloucky, and P. Varga, Surf. Sci. **424**, L321 (1999).
[10] M. Kiguchi, S. Entani, K. Saiki, H. Inoue, and A. Koma, Phys. Rev. B **66**, 155424 (2002).
[11] J. Kramer, C. Tegenkamp, and H. Pfnür, J. Phys.: Condens. Matter **15**, 6473 (2003).
[12] M. Pivetta, H.-C. Ploigt, F. Patthey, and W.-D. Schneider (unpublished).
[13] P. M. Echenique and J. B. Pendry, J. Phys. C **11**, 2065 (1978).
[14] R. Fischer, S. Schuppler, N. Fischer, Th. Fauster, and W. Steinmann, Phys. Rev. Lett. **70**, 654 (1993).
[15] U. Höfer, I. L. Shumay, Ch. Reuss, U. Thomann, W. Wallauer, and Th. Fauster, Science **277**, 1480 (1997).
[16] G. Binnig, K. H. Frank, H. Fuchs, N. Garcia, B. Reihl, H. Rohrer, F. Salvan, and A. R. Williams, Phys. Rev. Lett. **55**, 991 (1985).
[17] T. Jung, Y. W. Mo, and F. J. Himpsel, Phys. Rev. Lett. **74**, 1641 (1995).
[18] K. Bobrov, A. J. Mayne, and G. Dujardin, Nature (London) **413**, 616 (2001).
[19] S. Schintke, S. Messerli, M. Pivetta, F. Patthey, L. Libioulle, M. Stengel, A. De Vita, and W.-D. Schneider, Phys. Rev. Lett. **87**, 276801 (2001).
[20] L. Bartels, S. W. Hla, A. Kühnle, G. Meyer, K.-H. Rieder, and J. R. Manson, Phys. Rev. B **67**, 205416 (2003).
[21] P. Wahl, M. A. Schneider, L. Diekhöner, R. Vogelgesang, and K. Kern, Phys. Rev. Lett. **91**, 106802 (2003).
[22] R. Bennewitz, M. Bammerlin, M. Guggisberg, C. Loppacher, A. Baratoff, E. Meyer, and H.-J. Güntherodt, Surf. Interface Anal. **27**, 426 (1999).
[23] Ch. Loppacher, U. Zerweck, and L. M. Eng, Nanotechnology **15**, S9 (2004).
[24] D. C. Marinica, C. Ramseyer, A. G. Borisov, D. Teillet-Billy, J. P. Gauyacq, W. Berthold, P. Feulner, and U. Höfer, Phys. Rev. Lett. **89**, 046802 (2002).

[25] M. Machado, E. V. Chulkov, V. M. Silkin, U. Höfer, and P. M. Echenique, Prog. Surf. Sci. **74**, 219 (2003).
[26] Y. Wang and J. P. Perdew, Phys. Rev. B **44**, 13298 (1991).
[27] P. E. Blöchl, Phys. Rev. B **50**, 17953 (1994).
[28] C. J. Fall, N. Binggeli, and A. Baldereschi, Phys. Rev. Lett. **88**, 156802 (2002); Phys. Rev. B **66**, 075405 (2002).
[29] J. VandeVondele and A. De Vita, Phys. Rev. B **60**, 13241 (1999).
[30] F. E. Olsson and M. Persson, Surf. Sci. **540**, 172 (2003).